X-ray thin-film measurement techniques
IV.   In-plane XRD measurements

Shintaro Kobayashi*

1.   Introduction

X-ray diffraction intensities from a thin film deposited on a substrate can be relatively weak in comparing to the enormous X-ray diffraction and background intensities from its substrate. The in-plane XRD technique with a grazing incident x-ray beam has been used successfully to enhance the thin-film intensities and to minimize the substrate intensities in the analysis a thin-film[1].

Three-dimensional thin-film structure, such as preferred orientation (or texture), orientational relationship and lattice distortion between an epitaxial film and its substrate, crystallite-size anisotropy, etc, can be obtained from both in-plane and out-of-plane XRD measurements (see the second review of this series[2]). It is well known that the crystalline structure of a thin film can affect the device characteristics.

In this article, the in-plane XRD technique used for the characterizations of extremely thin films as well as the crystallinity and orientational relationships in complex heteroepitaxial systems is explained.

2.   What is in-plane XRD?

In-plane XRD is a technique used for measuring diffraction intensities from lattice planes normal to the surface of a sample (Fig. 1).

Four typical characteristics of in-plane XRD are:
1. Diffraction from the lattice planes normal to the surface of a sample can be observed.
2. Diffraction from an extremely thin film can be detected.
3. Diffraction and background intensities from the substrate can be minimized.
4. A nondestructive depth-profile analysis is possible by using various angles of the incident X-ray beam.

The geometrical layouts of symmetrical, asymmetrical (thin film method) and in-plane XRD measurements are summarized in Fig. 1. The scattering vector (the normal vector of the lattice planes) in an out-of-plane measurement is pointed out from the sample surface, whereas the scattering vector lies parallel to the thin-film surface in the case of an in-plane XRD measurement. In other words, in-plane XRD is a technique for measuring lattice planes normal to the surface of a thin film.

In a symmetric out-of-plane XRD measurement, the incident angle is normally large and the incident X-rays will penetrate deep inside a sample. Therefore, XRD

intensities from an ultra thin film will not easily be detected with this technique. On the other hand, a grazing-incident X-ray beam is employed in an in-plane XRD measurement (bottom graph of Fig. 1) so that the incident X-ray beam travels a long distant inside the thin film, and thus high diffraction intensities from the film can be obtained.

More information on the angle of the incident X-ray beam and its penetration depth are reported next. The angle of the incident X-ray beam can be controlled independently on the sample rotation angle (φ) and the position of the detector ($2\theta\chi$) as shown in the geometry of the in-plane XRD measurement (see the bottom graph of Fig. 1). The penetration of an incident X-ray beam
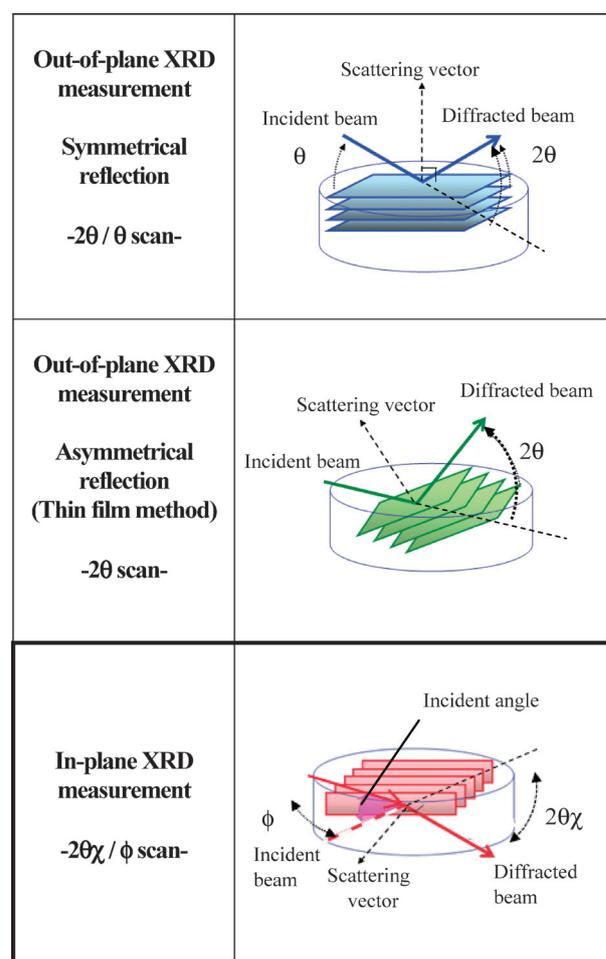
Fig. 1.   Geometries of out-of-plane and in-plane XRD measurements.

* Application Laboratory, Rigaku Corporation.
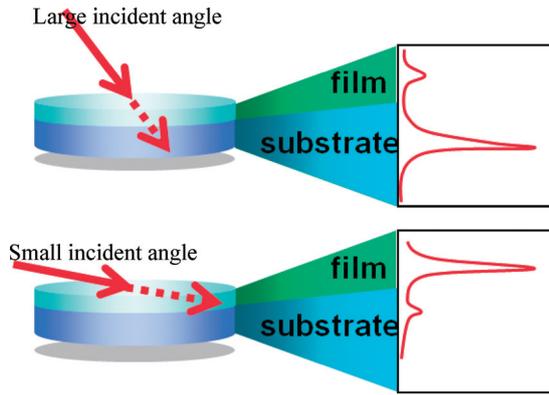
Fig. 2. Schematic drawings of diffraction intensities from a thin film deposited on a substrate with different incident angles.

into a sample is deep when the incident angle is large, whereas the penetration depth can be extremely shallow for a very small incident angle (see Fig. 2). Therefore, the in-plane XRD technique using a number of different incident angles can be used for an effective and non-destructive structure-depth analysis of a thin film.

3. Characteristics of in-plane XRD

When the sample surface is flat and the incident angle is extremely small, the incident X-rays can be totally reflected, because the refractive index of a material is smaller than unity. By increasing the incident angle over a certain value, the incident X-ray can penetrate deep into a sample. This angle is known as the critical angle for the total external reflection (θ_c), which is a function of the wavelength of the incident X-rays and the density of the material.

At around the critical angle, a part of incident X-ray beam is reflected on the sample surface, and the rest of X-ray beam penetrates into the sample. The penetrated X-ray beam propagates almost parallel to the sample surface, because the incident angle of the X-ray beam is extremely small, and also the penetrated X-ray beam is refracted so as to propagate along the sample surface. The penetrated X-ray beam will come out from the sample surface by diffraction from lattice planes either inclined or perpendicular to the sample surface, known as out-of-plane asymmetrical reflection (middle graph of Fig. 2) or in-plane XRD (bottom graph of Fig. 2), respectively.

The penetration depth (t) of an incident X-ray beam as a function of the incident angle of α (this angle is controlled by the motion of ω-axis of a goniometer) can be roughly estimated from the following equation[2]:

$$t = \frac{4.61}{2\mu} \cdot \sin \alpha \quad (1)$$

α: Incident angle of X-rays
μ: Liner absorption constant of X-rays

If the incident angle, α, is very small, and is close to the critical angle for the total external reflection, the

contribution of the reflection and refraction phenomena should be taken into consideration, then, Eq. (1) is no more valid. For the case around the critical angle, the penetration depth of X-ray (t_{tot}) can be calculated using the following equation:

$$t_{tot} = \frac{1}{\sqrt{2} \cdot \frac{2\pi}{\lambda} \cdot \left[\sqrt{(\theta_c^2 - \alpha^2)^2 + 4\beta^2} + \theta_c^2 - \alpha^2 \right]^{1/2}} \quad (2)$$

$$\beta = \frac{\lambda}{4\pi} \mu$$

λ: Wavelength of X-rays
θ_c: Critical angle for the total external reflection

Using Eq. (2), the penetration depth t_{tot} as a function of the incident angle can be calculated. Calculated values of t_{tot} and the CuKα X-ray reflectivity (i.e., ratio of reflection intensity to the incident X-ray intensity) profiles as a function of the incident angle α for Si, Cu and Au are plotted in Fig. 3. Drastic changes of the penetration depths occur at the incident angles close to the critical angles for the total external reflection of these materials.

Figure 4 shows an example of the variations of the in-plane XRD intensity diffracted by a Si film as a function of the incident angles. The critical angle for Si (0.23°) is indicated with an arrow in Fig. 4, and it should be noted that the maximum Si intensity occurs at the incident angle slightly larger than the critical angle. This can be explained as follows:

When the incident angle is slightly below the critical
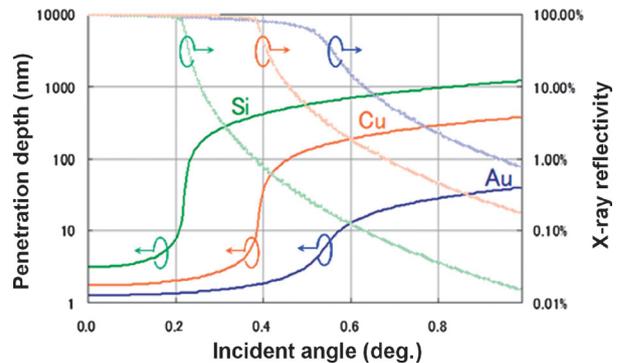
Fig. 3. Penetration depth and X-ray reflectivity around critical angles for total external reflection.
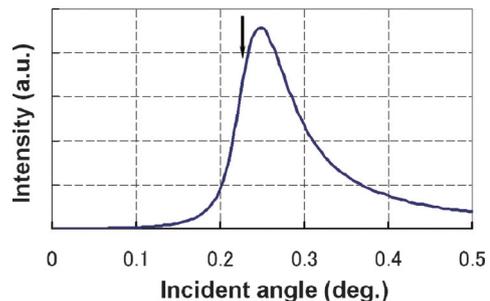
Fig. 4. Diffraction intensity *vs.* incident angle for Si.

angle, X-rays cannot penetrate deep inside the sample, and instead it travels parallel to the sample surface as an evanescent wave. Thus the sample volume contributing to in-plane diffraction is very limited , and thust the diffraction intensities are very weak.

In-plane XRD intensity increases with increasing incident angle around the critical angle, mainly due to the increase of sampling volume participating to in-plane XRD as shown in Fig. 3.

With further increase in the incident angle, the attenuation of the diffraction intensity caused by mass absorption gradually becomes dominant, and the in-plane XRD intensity diminishes monotonously. The competition between an increase in sampling volume and the attenuation of the diffraction intensity due to mass absorption results in the intensity maximum at the incident angle of slightly larger than the critical angle.

Figure 4 also shows the magnificent sensitivity of the intensity variation with the incident angle, proving that the divergence of the incident beam is less than 0.1° (along the surface normal direction).

In the next section, the optical systems employed for in-plane XRD measurements are discussed.

4. Optical systems used in in-plane XRD measurements

As discussed above, the collimation of the incident X-ray beam is very important for in-plane XRD. Conventional incident X-ray optics with multiple narrow slits can also be used for in-plane XRD, but the diffraction intensities from a thin film are mostly very weak. Figure 5 shows two of the most effective X-ray optical systems used for collimating and monochromatizing an incident X-ray beam, i.e. "parabolic multilayer mirror+parallel slits" and "polycapillary lenz". The former uses a line X-ray source, and the latter uses a point X-ray source to obtain an incident X-ray beam with equal vertical and horizontal divergences of about 0.3° (see right-hand side of Fig. 5).

The optical system using a parabolic multilayer mirror and parallel slits is shown in the left-hand side of Fig. 5. The parabolic multilayer mirror acts as a monochromator for CuKα radiation and also acts as a collimator to produce a parallel incident beam with a vertical divergence of around 0.05°. A smaller divergence can also be achieved by inserting a channel-cut monochormator together with the parallel slits. The collimation in this optical system is realized in the direction perpendicular to the long axis of the line X-ray source. Thus, a sample is mounted horizaontally so that this long axis is parallel to the surface of a sample. The detector is scanned in the horizaontal plane to record diffraction intensities from the sample, which is along the direction perpendicular to the tracking circle of the 2θ-axis motion. This is the reason why Rigaku SmartLab in-plane system is equipped with an additional 5th goniometer axis, $2\theta\chi$ (Fig. 6, this axis is called the in-plane axis). Details of the goniometer used in SmartLab have been previously described in the first review article of the series on X-ray thin-film measurement techniques[3].

As shown in the left-hand side of Fig. 5, the horizontal divergence of 0.1 to 1.0° for the incident X-ray beam can be obtained using an in-plane parallel slit collimator (In-plane PSC). Resolution of 0.1 to 1.0° for the receiving optic system is controlled by an in-plane parallel slit analyzer (In-Plane PSA), while receiving slits 1 and 2 are left wide-open during an in-plane XRD measurement.

Care must be taken to avoid the possibility that the incident X-ray beam may spill over the entire length (or width) of the sample at all incident angles in an in-plane XRD measurement.

The length, W, of the incident X-ray beam projected onto the sample surface depends on the width of the
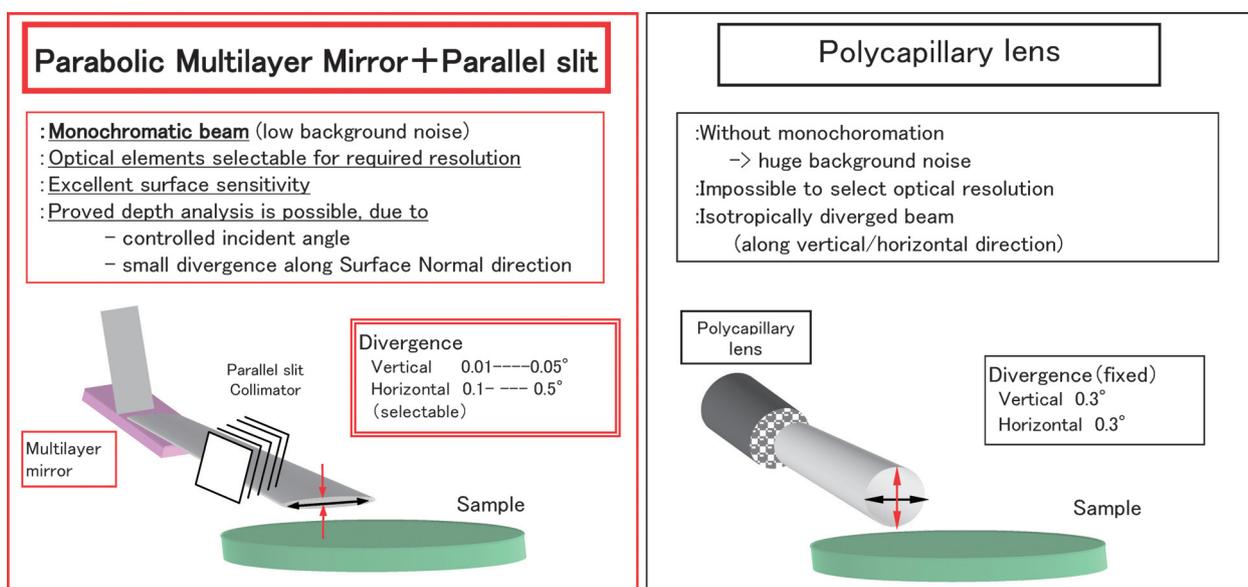
Fig. 5. Comparison of incident optics for in-plane XRD measurements.
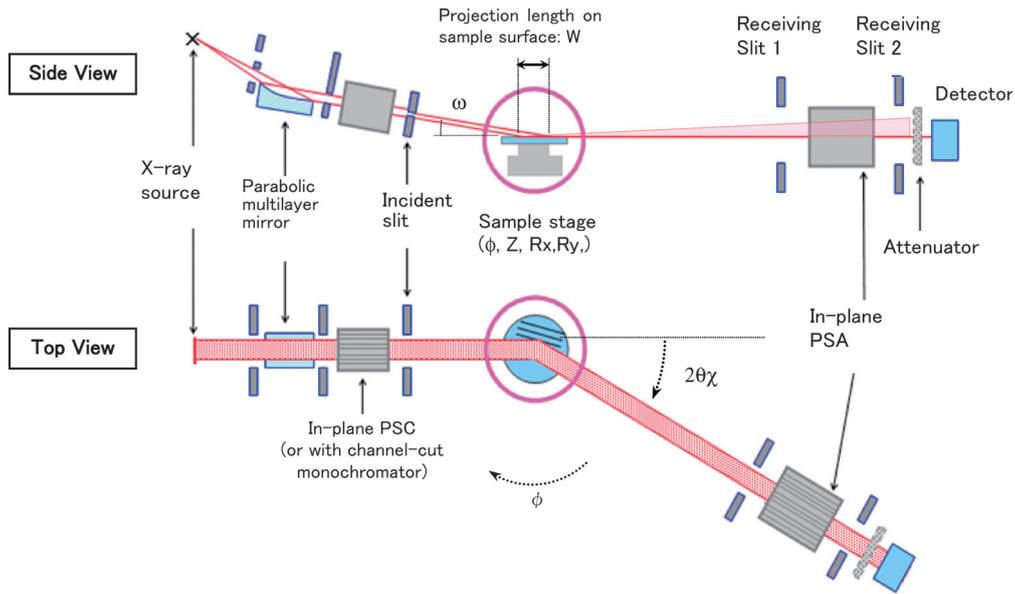
Fig. 6. In-plane XRD geometry of "SmartLab™".

incident beam sit and the incident angle of the incident X-ray beam. The value of W can be calculated as follows:

$$W\,(\mathrm{mm})=W_{\mathrm{IS}}\,(\mathrm{mm})/\sin\alpha \qquad (3)$$

W_{IS} (mm): Width of the incident slit
α (deg.): Incident angle

Values of W will be much larger that of W_{IS} when the incident angle is very small. For examples with a commonly used incident slit with $W_{\mathrm{IS}}=0.1\,\mathrm{mm}$, the projection length, W, are 23 and 11.5 mm for incident angles of 0.25° and 0.50°, respectively.

5. Useful methods and practices in in-plane XRD

In order to realize and utilize the surface-sensitive features of in-plane XRD measurements, optical systems used for in-plane diffraction experiments were described in section 4. Useful methods and practices in in-plane diffraction are discussed in this section.

5.1. Proper alignment of sample surface

An in-plane XRD measurement is very sensitive to the angle of the incident X-ray beam, which strikes the sample surface at a very shallow angle. During an in-plane XRD experiment, the incident angle of the X-ray beam must be kept constant, and the sample surface normal through the center of the sample must be properly aligned and coincident with the ϕ rotation axis of the goniometer[1],[3],[4].

The sample stage used in an in-plane XRD experiment should have a ϕ axis for the sample rotation about its center, a z axis for the sample height adjustment and also two orthogonal tilt-adjustment axes (see Rx and Ry in Fig. 7). Using the Rx and Ry axes, the sample surface normal can be precisely aligned with the ϕ rotation axis so that a precession motion of surface
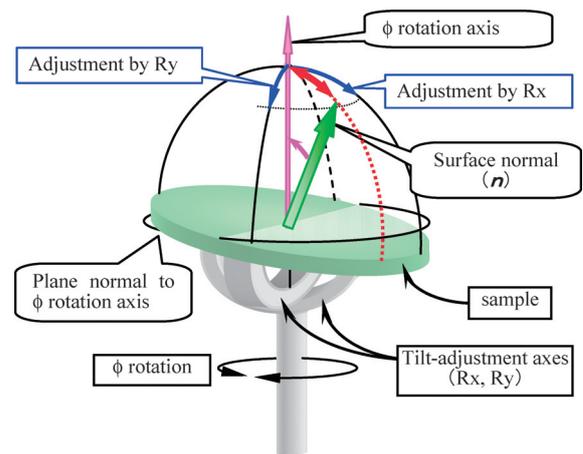
Fig. 7. A schematic figure for sample alignment mechanism using orthogonal Tilt-adjustment axes, Rx and Ry.
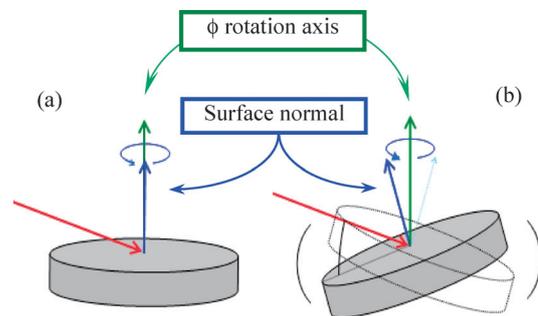
Fig. 8. Explanation of the precession motion of a sample by the rotation around ϕ axis.

(a) No precession motion by complete tilt alignment

(b) Precession motion caused by incomplete tilt alignment

normal vector during sample rotation can be avoid. An automatic sample-alignment software package is commonly installed in a commercially available in-plane

XRD system, and this software relieves a user from complex operation procedures.

By alternative uses of the Rx and Ry axes, it is possible to align the sample rotation axis to the crystallographic axis of an epitaxial film or its substrate. By analyzing the Rx and Ry values after these alignments, misorientation between substrate surface plane and lattice plane, or misorientation between substrate lattice planes and those of the epitaxial film can be calculated.

5.2. In-plane and pseudo in-plane geometries

Two different measurement geometries can be used in an in-plane XRD diffractometer. One of the geometries is using the in-plane $2\theta\chi$ axis and a horizontal sample as explained in the previous section, which is a main subject of this article. Another geometry is using the $2\theta/\omega$ axis (commonly used in an out-of-plane measurement) and a titled sample. The former is known as an in-plane XRD measurement, and the latter is called a pseudo in-plane XRD measurement. Geometries for these two sample placements are shown in Figs. 9 and 10.

It is possible to use a θ–θ goniometer system equipped with an in-plane $2\theta\chi$ axis to perform an in-plane XRD measurement and an out-of-plane XRD

Fig. 9. In-plane XRD geometry using in-plane axis.

Fig. 10. Geometry of *pseudo* in-plane XRD measurement.

measurement, while keeping the surface of a sample set in a horizontal plane. The θ–θ goniometer system has many advantages. For example, since a sample is kept horizontally, there is no need to worry about sample constraints caused by sample clamping during a high-temperature measurement using a heating stage.

In the pseudo in-plane XRD geometry, a sample should be tilted about 90° with the χ-axis taking a skew geometry. So, it is necessary to fix the sample, but the $2\theta/\omega$ axis is possible to be used for measurements as is done in an out-of-plane measurement. Moreover, a high-resolution in-plane XRD measurement of a sample can be performed by utilizing optical elements such as a channel-cut crystal monochromator and an analyzer crystal. However, in the pseudo in-plane XRD geometry, a commonly used line-focused X-ray source does not work well, because only a small part of incident X-rays for the line source will contribute to in-plane XRD. In view of this drawback, Rigaku Corporation manufactures the "SuperLab™" system that has high-flux brilliant point optics with confocal mirror systems, and this system can be used to measure both out-of-plane XRD and in-plane XRD measurements with ultra high resolution[5]–[7].

Either one of the two geometries (Figs. 9 and 10) can be used in a "SmartLab™"system. For measuring weak diffraction intensities from a thin film, the in-plane XRD geometry using the in-plane $2\theta\chi$ axis is recommended. For a high-resolution measurement (for example, resolution better than 0.1°), the pseudo in-plane XRD geometry is recommended.

5.3. Detector position (2θ axis)

In an in-plane XRD measurement (Fig. 9), the detector position is controlled by both the 2θ axis and the $2\theta\chi$ axis, and the measurements are performed by scanning the $2\theta\chi$ axis. Then, one may wonder where the 2θ axis should be positioned? The answer is "should be positioned at the same angle with the ω axis and fixed".

If the 2θ axis is positioned at an angle twice of that of the ω (or θ) axis similar to a $2\theta/\theta$ measurement, the $2\theta\chi$ axis tracks a circle obliquely inclined to the sample surface as shown in the upper graph of Fig. 11. Therefore, the exit angles of diffracted X-ray (see blue arrows in Fig. 11) will not be constant through the movement of $2\theta\chi$. The exit angle is maximum at $2\theta\chi=0°$, monotonously decreases to 0 at $2\theta\chi=90°$, and goes down to a minus value at $2\theta\chi >90°$. On the other hand, if the 2θ axis position is set at the same value as that of the ω axis, the exit angle of diffracted X-ray can be kept constant through the entire $2\theta\chi$ motion, ensuring that an in-plane XRD measurement can be performed under the same condition. This is the reason why the 2θ axis should be positioned at the same angle as that of the ω axis and be fixed for an in-plane XRD measurement.

5.4. In-plane rocking-curve measurements

In the second review article of this series[2], it was explained that the degree of preferred orientation
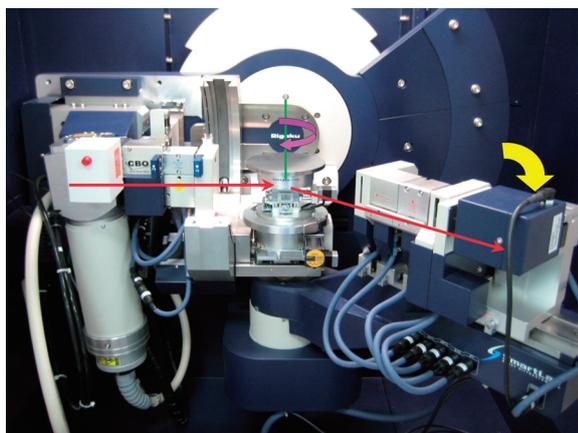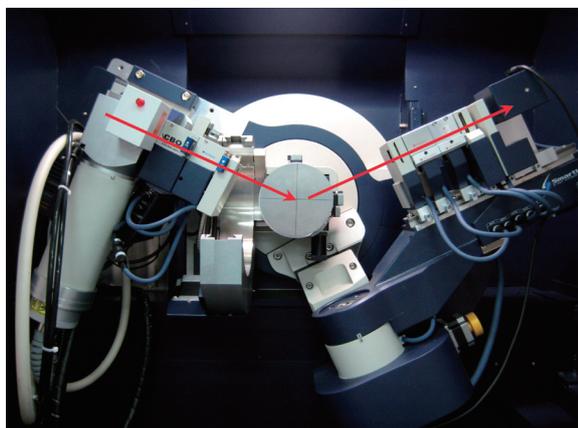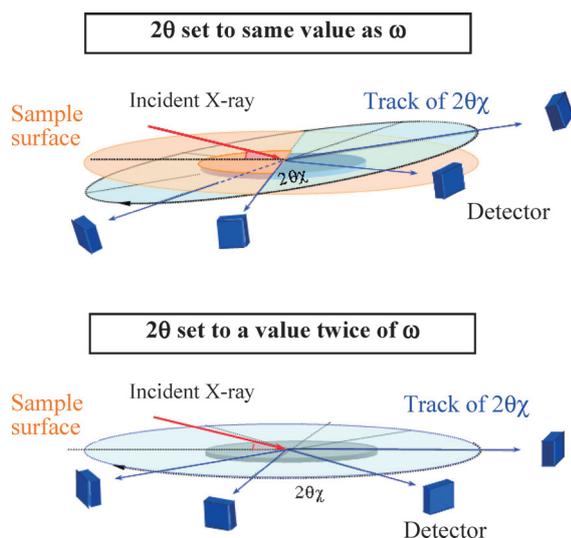
Fig. 11. Tracks of $2\theta\chi$ motion during an in-plane XRD.
Up: 2θ position is set to same value as ω
Down: 2θ position is set to a value twice of ω
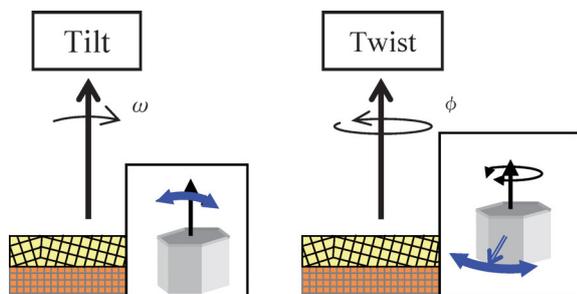
Fig. 12. Mosaic spread of Tilt/Twist distribution, and the corresponding sample-rocking axes.

(or texture) of a thin film can be analyzed from the width of an ω-scan rocking curve of an out-of-plane XRD measurement. Similarly, the degree of preferred orientation within a sample surface can be analyzed by a ϕ-rocking scan in an in-plane XRD measurement with the detector being fixed at a $2\theta\chi$ position for a diffraction peak of interest.

The quality of an epitaxial thin film is normally evaluated from mosaic spread along the film-growth direction that is known as tilt distribution (or simply tilting as shown in the left–hand side of Fig. 12). With the advances in thin-film growth techniques, heteroepitaxial growths of highly mismatched films on substrates (for example, GaN film on sapphire substrate) are now widely investigated. The lattice alignment of an epitaxial film with its substrate becomes an important parameter for elucidating the nature of an epitaxial-growth process. The degree of mosaic spread within the surface plane is called "twist distribution (or simply twisting)", and it can be easily and directly characterized form a ϕ-rocking scan in an in-plane XRD measurement as shown in the right-side side of Fig. 12.

5.5. In-plane XRD measurement of a small sample

Here is a brief discussion of the case of measuring a small sample.

Ideally, a sample with a large surface area is desirable for an in-plane XRD measurement so that the incident X-ray beam will not spill over the sample surface during the entire measurement. The incident X-ray beam normally has a rectangular shape. One side of the rectangle is equal to the projected length of W (see Fig. 6), and the length of the other side of the rectangle is fixed by the height of the limiting incident slit. For a small square sample with 10-mm long edges, the size and the shape of the sample will match the length of the incident X-ray beam projected onto the sample surface when a 10-mm height limiting incident slit is employed. However this shape-matching can be maintained only at $\phi=0$, 90, 180 and 270°, but not at other ϕ angles. Therefore, intensity normalization as a function of the ϕ position may be required for a quantitative in-plane XRD analysis. In addition when the incident X-ray beam spills over a small sample surface during an in-plane measurement, the incident X-ray beam may strike the sidewalls (or edges) of the film and/or its substrate. This may produce undesirable X-rays recorded by the detector.

6. Applications of in-plane XRD
6.1. Characterization of an ultra thin monolayer organic film

The first example is the application of in-plane XRD for the analysis of an organic Langmuir–Blodgett thin film of monolayer thick grown on a Si substrate[8]. The film thickness was determined to be 1.7 nm by the X-ray reflectivity method (details of the X-ray reflectivity method will be described in the next review article of this series), and this thickness agrees with the length of a single molecular chain of the organic molecule, confirming monolayer growth of the organic film. The in-plane XRD pattern is shown in the left-hand side of Fig. 13, and the d-spacing for the peak at 21° of 2θ is 0.42 nm, corresponding to the lattice spacing of honeycomb surface lattice formed by the chain molecules.

The in-plane XRD measurement technique has
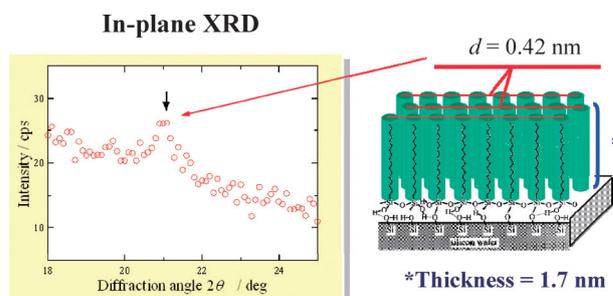
Fig. 13. Example of In-plane XRD analysis; a monolayer organic thin film.
Left: In-plane XRD profile
Right: Molecular structure model

been used successfully for the characterization of various functional thin films such as transparent conductive oxide (TCO) films[9]–[12],[30], magnetic thin films[13]–[15], compound semiconductors[5],[16]–[18],[29], organic thin films[19],[22],[31], high-k materials[23],[24], and superconductive epitaxial thin films[25].

6.2. Characterization of a polycrystalline thin film by in-plane and out-of plane XRD

Another example is the characterization of a polycrystalline Si thin film (50 nm thick) on a glass substrate by in-plane and out-of-plane XRD.

As shown in Fig. 14(a), only a strong diffraction peak of Si (111) can be observed in the out-of-plane XRD pattern, showing a strong [111] preferred orientation (or texture) presented in the film.

On the other hand, strong Si 220 and 422 peaks (marked with red arrows in Fig. 14(b)) are observed in the in-plane XRD pattern shown in Fig. 14(b), because the intensities of these peaks were enhanced due to the contributions from the Si $(2\bar{2}0)$ and $(4\bar{2}\bar{2})$ planes, respectively, which are perpendicular to the (111) surface. Si 111, 311, 400 and 331 diffraction peaks also appear in the in-plane XRD pattern (see blue arrows in Fig. 14(b)), and this indicates that the [111] texture presented in this polycrystalline film has a certain amount of tilting breadth, and this [111] orientation spread made possible the detection of in-plane diffraction peaks from the Si $(11\bar{1})$, $(3\bar{1}\bar{1})$, (400) and $(\bar{3}31)$ lattice planes.

As stated earlier in section 6.2, the thickness of the polycrystalline Si film deposited on a glass substrate is 50 nm. Even for such a thin film, strong diffraction peaks from the film and only minimum background from the
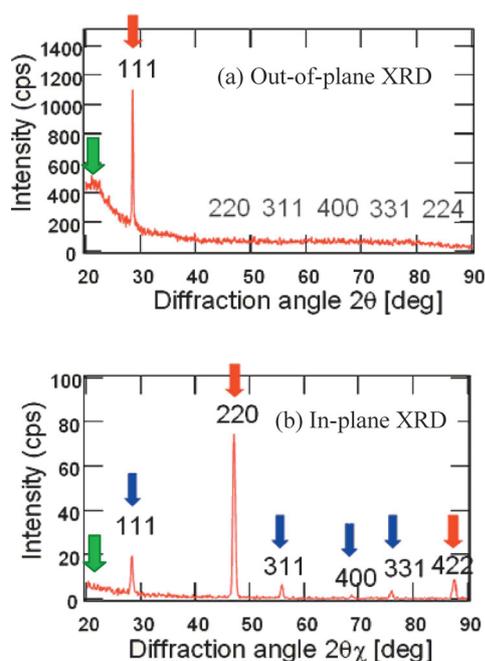
glass substrate were detected by in-plane XRD (the strongest background from the glass substrate is marked with green arrows in Figs. 14(a) and 14(b)).

By a combination of in-plane and out-of-plane XRD measurements, a three-dimension thin-film structure, including lattice distortion, crystallite sizes, preferred orientation (including their anisotropy between the growth direction and the direction within surface plane) in a sample can be obtained.

6.3. Structural depth-profile analysis

Seven in-plane XRD patterns for a (Pb, La)TiO$_3$ (PLT) film (250 nm thick) on a Pt film(150 nm) over a Si substrate recorded with increasing incident angles from $\omega = 0.4$ to $1.0°$ with the step of $\Delta\omega = 0.1°$ are shown in Fig. 15. This figure shows that the Pt 220 peak intensity from the intermediate Pt layer increases with increasing incident angle (ω), and this is because the incident X-ray beam traveled longer inside the intermediate Pt layers as the incident angle increased from 0.4 to 1.0°.

Recently, there is increasing interest in the use of the in-plane XRD technique, mainly because of the large X-ray penetration depths, which make possible the study of buried interfaces and layers in a sample. This feature is unattainable with the electron diffraction technique. The structure characterization of thin films is often desirable to be done in a nondestructive way, because the process or sample treatment likes peering off the top layers or thinning down for a TEM observation may change the sample conditions or relieve the strains stored at the interfaces. Using the in-plane XRD technique, buried interface and layers can be analyzed nondestructively[26].

6.4. In-plane orientation evaluations

Figure 16 shows two in-plane rocking-curve patterns of an epitaxial and a non-epitaxial PLT films. The in-plane rocking curve of the PLT 101 reflection from the

Fig. 14. XRD profiles of polycrystalline Si thin film.
(a) Out-of-plane XRD measurement
(b) In-plane XRD measurement
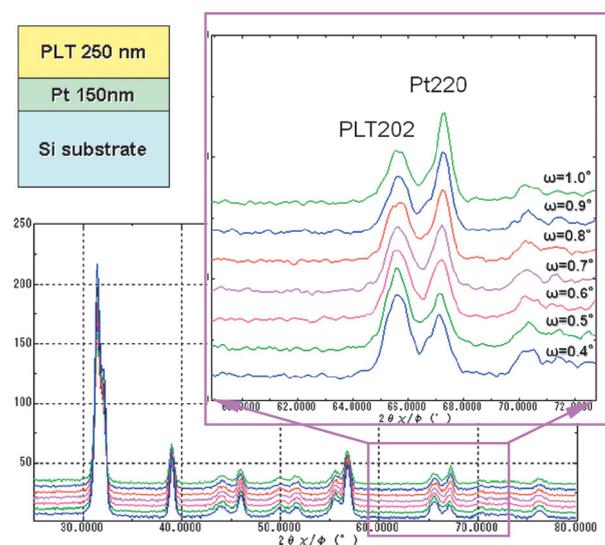
Fig. 15. In-plane XRD profiles of PLT/Pt thin film on Si substrate measured with different incident angles (ω).
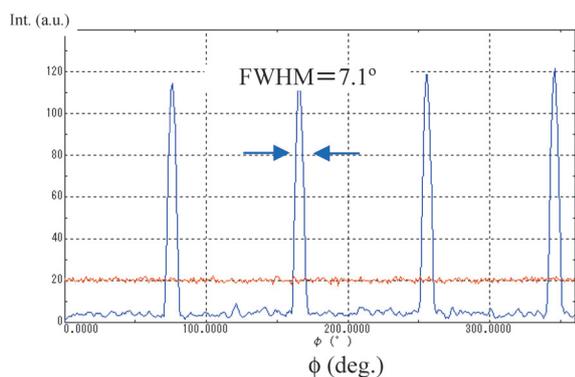
Fig. 16. In-plane rocking curve patterns of an epitaxial and a non-epitaxial PLT films. The blue XRD pattern is for the epitaxial film, and the red curve is for the non-epitaxial film with random in-plane orientation.

Fig. 17. Twist breadths of NdF_3 epitaxial films with different thickness and growth temperature.

epitaxial PLT film is shown in the blue curve of Fig. 16. The red curve in Fig. 16 is the rocking curve for the non-epitaxial PLT film with random in-plane orientation.

The in-plane rocking-curve pattern for the epitaxial PLT film has four sharp peaks with 90° intervals showing four-fold symmetry within the surface plane. The observed four-fold symmetry was generated by the c-axis of the tetragonal PLT film grown perpendicular to its substrate. The degree of twisting of the epitaxial PLT film calculated from the full width at half maximum (FWHM) of the peak is 7.1°. The azimuth positions of these four peaks matched with those of [001] axis of the substrate lattice.

On the other hand, in-plane diffraction intensities from a PLT film with random in-plane orientation remain essentially constant and are independent of the azimuthal direction. It should be noted that the observed in-plane diffraction intensities are significantly higher than those of the background intensities.

The next example is on the crystallinity analysis of six NdF_3 thin films epitaxially grown on Si (111) substrates. Values of six twist breadths for the NdF_3 thin films grown at three different growth temperatures of 400, 550 and 700°C with thicknesses of 40 and 300 nm are plotted in Fig. 17. Although the NdF_3 films grown at 400 and 550°C show improvements in the twist breath and thus crystallinity as the films grew from 40-nm to 300-nm thick, degradation in the 300-nm thick film was found from the increases in the value of the twist breadth for the film grown at 700°C. The differences in crystallinity can be correlated with the differences in the growth modes, as that the growth is predominant by the island growth mode at temperatures lower than 600°C and by the spiral growth mode at temperatures higher than 600°C[27]–[28].

When an epitaxial film is to be analyzed using the in-plane XRD technique, a referential azimuth direction must first be determined. The referential azimuth direction must be defined with crystallographic axes of the substrate, since the process of growing an epitaxial film is to rearrange the atoms in the film to match the atomic arrangements on the surface of its substrate.
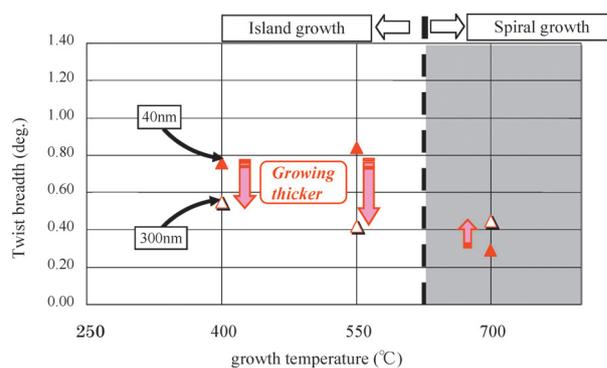
After defining the referential azimuth direction, the analysis of lattice planes of an epitaxial film will be done by making in-plane $2\theta\chi/\phi$ scans to determine the degree of match between the epitaxial film and its substrate.

The observed in-plane XRD peak positions and consequently values of lattice constants of an epitaxial film may be different from those reported in literatures, because the epitaxial growth of a film can cause lattice distortion in the film. It should also be noted that an in-plane XRD pattern of an epitaxial film may have more than one set of diffraction peaks from different sets of (hkl) lattice planes, suggesting the presences of multiple domains in the epitaxial film. It is also useful to measure the values of twist breadths of these domains. If an in-plane reciprocal space map (RSM) measurement is performed, the degrees of twist and the characteristics of these domains together with the azimuth orientation relationship between the film and its substrate can be determined directly from the RSM[26],[29]–[31].

The "in-plane lattice misorientations" in complex epitaxial films or large mismatching systems are currently popular research topics[32]. An extremely small misorientation of less than 1° between an epitaxial film and its substrate can be detected either from an in-plane rocking curve or from an in-plane RSM.

7. Conclusions

Details of the in-plane XRD technique and its applications to characterizing thin films have been discussed. Using the in-plane XRD technique, information on lattice planes perpendicular to the surface of a sample can be obtained, and the diffraction intensities from an extremely thin film can also detected. In addition, three-dimension thin-film structure information, such as lattice distortion, crystallite sizes, azimuth-orientation alignment/distributions, etc. in a sample can be obtained by analyzing both in-plane and out-of-plane XRD data. By controlling the angle of the incident X-ray beam, a nondestructive depth-profiling analysis is also possible using in-plane XRD.

As discussed above, an analysis of thin-film diffraction peaks obtained by in-plane and/or out-of-plane XRD can provide detailed structural information

of a film. On the other hand, information on layer thickness, density and roughness of layer interfaces, etc. can be obtained by the X-ray reflectivity (XRR) method. In the next review article of the series on X-ray thin-film measurements, details of the XRR method will be discussed.

References

(1) K. Omote, and J. Harada: *Advances in X-ray Analysis*, **43** (2000), 192–200.

(2) T. Mitsunaga: *Rigaku Journal*, **25** (2009), No. 1, 7–12.

(3) K. Inaba: *Rigaku Journal*, **24** (2008), No. 1, 10–15.

(4) D. Guo, S. Ikeda, K. Saiki, H. Miyazoe and K. Terashima: *Jour. Appl. Phys.,* **99** (2006), 094502-1–094502-7.

(5) K. Omote, H. Omi and T. Kawamura: *Trans. Mater. Res. Soc. Jpn.,* **33** (2008), 535–539.

(6) Y. Ito, K. Inaba, K. Omote, Y. Wada and S. Ikeda: *Jpn. Jour. Appl. Phys.,* **46** (2007), L773–L775.

(7) Y. Ito, K. Inaba and K. Omote: *Jour. Phys.: Conf. Ser.,* **83** (2007), 012015-1 - 012015-4.

(8) K. Kojio, A. Takahara, K. Omote and T. Kajiyama: *Langmuir,* **16** (2000), 3932–3936.

(9) T. Yamamoto, T. Yamada, A. Miyake, H. Makino and N. Yamamoto: *Jour. of SID,* **16** (2008), 713–719.

(10) T. Kawaharamura and S. Fujita: *Phys. Stat. Solidi-c,* **9** (2008), 3138–3140.

(11) T. Yamada, A. Miyake, S. Kishimoto, H. Makino, N. Yamamoto and T. Yamamoto: *Appl. Phys. Lett.,* **91** (2007), 051915-1–051915-3.

(12) H. Ohta, M. Orita, M. Hirano and H. Hosono: *Jour. Appl. Phys.,* **91** (2002), 3547–3550.

(13) A. Hirohata, H. Kurebayashi, S. Okamura, M. Kikuchi, T. Masaki, T. Nozaki, N. Nozaki and K. Inomata: *Jour. Appl. Phys.,* **97** (2005), 103714-1–103714-8.

(14) Z. L. Zhao, K. Inaba, Y. Ito, J. S. Chen, B. H. Liu, J. Ding and J. P. Wang: *Jour. Appl. Phys.,* **95** (2004), 7154–7156.

(15) S. Saito, N. Itagaki, F. Hoshi and M. Takahashi: *Jour. Appl. Phys.,* **93** (2003), 8182–8184.

(16) K. Kayanuma, H. Hiramatsu, T. Kamiya, M. Hirano and H. Hosono: *Appl. Phys. Lett.*, **88** (2006), 092106-1–092106-3.

(17) S. H. Park, T. Hanada, D. C. Oh, T. Minegishi, H. Goto, G. Fujimoto, J. S. Park. I. H. Im, J. H. Chang, M. W. Cho, T. Yao and K. Inaba: *Appl. Phys. Lett.,* **91** (2007), 231904-1–231904-3.

(18) K. Matsuzaki, H. Yanagi, T. Kamiya, H. Hiramatsu, K. Nomura, M. Hirano and H. Hosono: *Jour. Appl. Phys.,* **105** (2009), 073903-1–073903-7.

(19) Y. Zhang, K. Tajima and K. Hashimoto: *Macromolecules,* **42** (2009), 7008–7015.

(20) S. Ikeda, K. Saiki, Y. Wada, K. Inaba, Y. Ito, H. Kikuchi, K. Terashima and T. Shimada: *Jour. Appl. Phys.,* **103** (2008), 084313-1–084313-9.

(21) H. Yoshida, K. Inaba and N. Sato: *Appl. Phys. Lett.,* **90** (2007), 181930-1–181930-3.

(22) K. Fukuda, T. Sekitani and T. Someya: *Appl. Phys. Lett.,* **95** (2009), 023302-1–023302-3.

(23) P. Zaumseil and T. Schroeder: *Jour. Appl. Phys.,* **104** (2008), 023532-1–023532-7.

(24) M. Komatsu, R. Yasuhara, H. Takahashi, S. Toyoda, H. Kumigashira, M. Oshima, D. Kukuruznyak and T. Chikyow: *Appl. Phys. Lett.,* **89** (2006), 172107-1–172107-3.

(25) H. Hiramatsu, T. Katase, T. Kamiya, M. Hirano and H. Hosono: *Appl. Phys. Lett.,* **93** (2008), 162504-1–162504-3.

(26) Y. F. Chen, S. K. Hong, H. J. Ko, V. Kirshner, H. Wenish, T. Yao, K. Inaba and Y. Segawa: *Appl. Phys. Lett.,* **78** (2001), 3352–3354.

(27) J. M. Ko, S. D. Durbin, T. Fukuda, and K. Inaba: *J. Vac. Sci. Technol*., **B19**, (2001), 2007–2012.

(28) J. M. Ko, K. Inaba, S. D. Durbin, and T. Fukud: *Jour. Cryst. Growth,* **212** (2000), 155–160.

(29) T. Minegishi, J. H. Yoo, H. Suzuki, Z. Vashaei, K. Inaba, K. Shim and T. Yao: *Jour. Vac. Sci. Technol.,* **B23** (2005), 1286–1290.

(30) H. Ohta, M. Orita, M. Hirano and H. Hosono: *Jour. Appl. Phys.,* **89** (2001), 5720–5725.

(31) M. Ofuji, K. Inaba, K. Omote, H. Hoshi, Y. Takanishi, K. Ishikawa, and H. Takezoe: *Jpn. Jour. Appl. Phys.*, **41** (2002), 5467–5471.

(32) H. K. Chauveau, P. D. Mierry, H. Cabane and D. Gindhart: *Jour. Appl. Phys.,* **104** (2008), 113516-1–113516-8.